ACSNANO
www.acsnano.org
ARTICLE

All-Elastomer-Based Triboelectric Nanogenerator as a Keyboard Cover To Harvest Typing Energy

Shengming Li,[†,‡,⊥] Wenbo Peng,[‡,⊥] Jie Wang,[‡,⊥] Long Lin,[‡] Yunlong Zi,[‡] Gong Zhang,[†] and Zhong Lin Wang*[,‡,§]

[†]Department of Mechanical Engineering, Tsinghua University, Beijing 100084, China
[‡]School of Materials Science and Engineering, Georgia Institute of Technology, Atlanta, Georgia 30332-0245, United States
[§]Beijing Institute of Nanoenergy and Nanosystems, Chinese Academy of Sciences, Beijing 100083, China

Supporting Information

ABSTRACT: The drastic expansion of consumer electronics (like personal computers, touch pads, smart phones, *etc.*) creates many human−machine interfaces and multiple types of interactions between human and electronics. Considering the high frequency of such operations in our daily life, an extraordinary amount of biomechanical energy from typing or pressing buttons is available. In this study, we have demonstrated a highly flexible triboelectric nanogenerator (TENG) solely made from elastomeric materials as a cover on a conventional keyboard to harvest biomechanical energy from typing. A dual-mode working mechanism is established with a high transferred charge density of ∼140 $\mu C/m^2$ due to both structural and material innovations. We have also carried out fundamental investigations of its performance dependence on various structural factors for optimizing the electric output in practice. The fully packaged keyboard-shaped TENG is further integrated with a horn-like polypyrrole-based supercapacitor as a self-powered system. Typing in normal speed for 1 h, $\sim 8 \times 10^{-4}$ J electricity could be stored, which is capable of driving an electronic thermometer/hydrometer. Our keyboard cover also performs outstanding long-term stability, water resistance, as well as insensitivity to surface conditions, and the last feature makes it useful to research the typing behaviors of different people.

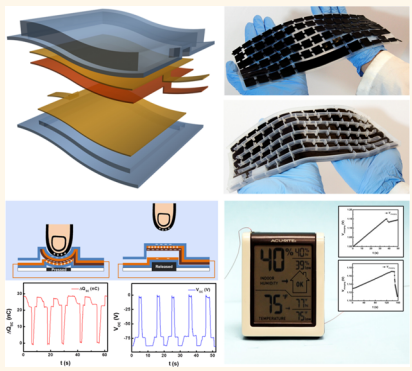

KEYWORDS: *biomechanical energy harvesting, triboelectric nanogenerator, elastomeric materials, keyboard cover, high flexibility*

In order to address the problem of increasing energy demand with limited traditional resources, exploring alternative energy sources from the ambient environment has drawn extensive attention.[1−8] Mechanical energy is one of the promising options especially for specific applications[5,6,9−14] for both large scope and microscale energy requirements.[15−21] Triboelectric nanogenerators (TENGs), featuring high energy harvesting efficiency, an unambiguous process route, low manufacturing cost, high system reliability and stability, and environmentally friendly materials, have been invented for mechanical energy harvesting from the ambient environment.[22−25] In recent decades, with the development of computer science and Internet technology, human−machine interfaces (HMIs) have been indispensable in our daily life, in the form of keyboards, buttons, and touch screens, *etc.* According to the statistics of American Population Characterization published in 2013, 75.6% of households reported that they are in possession of computers. During our interactions with computers, massive mechanical energy has been used for typing operations. By introducing TENGs to HMIs (especially keyboards) and integrating them with an appropriate energy storage unit, we are able to harvest part of the mechanical energy used for typing.[21,26] The as-designed self-powered system could be utilized to power consumer and personal electronics to replace batteries, which not only have limited lifetime but may also lead to environmental and safety issues.

To build a TENG-based self-powered system to harvest mechanical energy from the keyboard and other HMIs, there are some basic principles to consider: (1) The TENG should be highly adaptable to the keyboard. (2) The TENG integrated to the keyboard should not create extra effort to the operator. (3) The TENG should deliver high output power, making it possible to replace batteries. (4) The TENG should have features such as simple fabrication procedures, uncomplicated structure, and low cost. In this work, we present a highly

Received: June 14, 2016
Accepted: August 4, 2016

DOI: 10.1021/acsnano.6b03926
ACS Nano XXXX, XXX, XXX−XXX

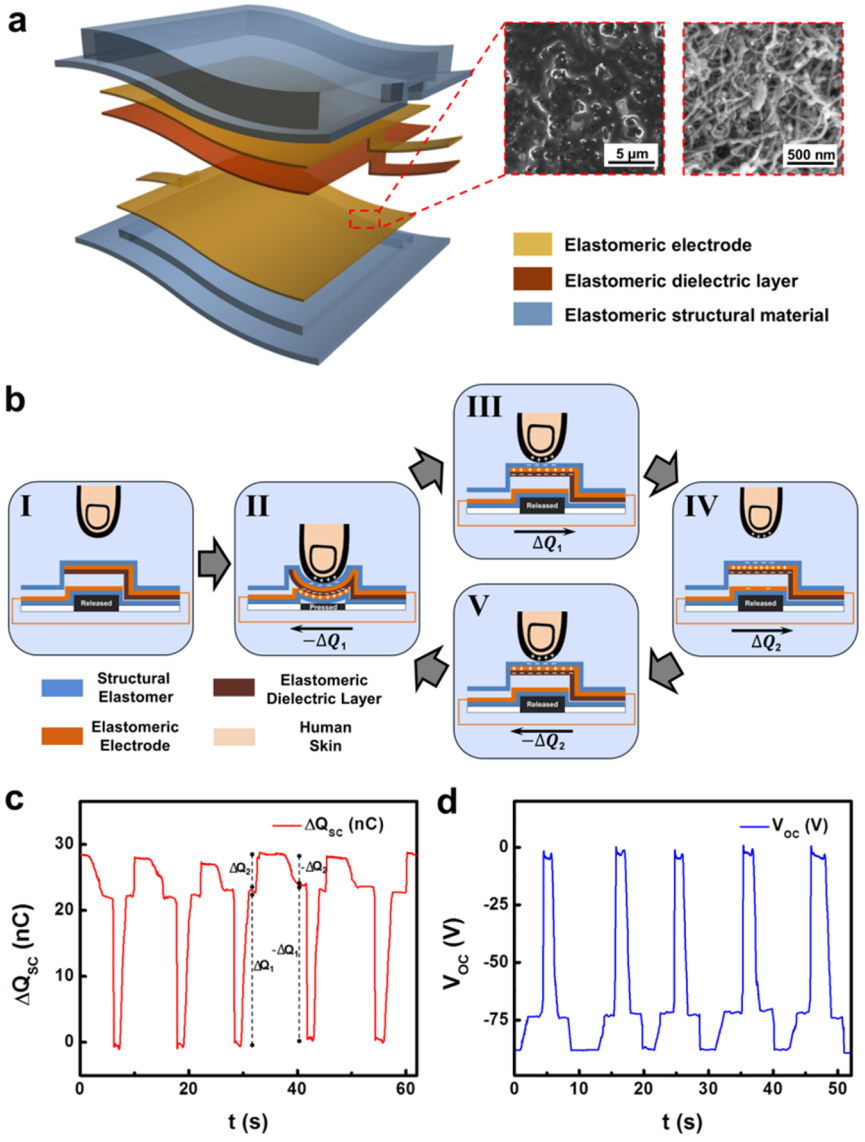

Figure 1. Basic structure, proposed working principle, and characteristic electric output of the dual-mode elastomeric TENG to harvest energy from a keyboard and buttons. (a) Schematic illustration showing the structure design of the elastomeric TENG. The inset on the left is a top-view SEM image of the dielectric layer, and the inset on the right is an SEM image of the CB/CNT mixture, which is the conductive ingredient of the elastomeric electrodes. (b) Schematic illustrations showing the proposed working principle of the elastomeric TENG, with the electron flow diagram in five consecutive states. Among them the last four states form a cycle. (c) $\Delta Q_{SC}-t$ curve by striking the TENG until maximum deformation with nitrile gloves on. (d) $V_{OC}-t$ curve by striking the TENG until maximum deformation with nitrile gloves on.

flexible TENG solely made by elastomeric films to harvest biomechanical energy efficiently in the form of a keyboard cover. Due to the material and structural innovation of this TENG, the above concerns have been addressed. First, solely fabricated by elastomeric silicone materials, the TENG renders high flexibility and stretchability.[27,28] These not only could facilitate the cover to adapt to the keyboard but also will not lead to higher workload. Second, benefiting from the flexible and stretchable layers for contact electrification, the tribo-charge density could be significantly improved because of more adequate contact. The structural design of the TENG is also optimized by incorporating the contact-separation mode and the single-electrode mode. This one-step further improves the electric output. Third, the structural and material factors to improve the feasibility of the TENG in real practice have also been studied and adjusted. Finally, we have fabricated one keyboard cover and built the corresponding self-powered system. We have proven that by harvesting mechanical energy purely from typing, an electronic device could be powered without an external power supply. Additionally, the keyboard cover is also featured with long-term stability, water resistance, and insensitivity to environmental factors and surface states.

RESULTS AND DISCUSSION

The basic structure of the TENG to harvest mechanical energy from the keyboard or buttons is schematically illustrated in Figure 1a (here, we exhibit the structure of TENG designed for one key, which could be developed into a complete keyboard cover or adjusted for the buttons with different shapes). The TENG was assembled with five layers of elastomeric films. The top and bottom layers were supporting structures produced by casting the platinum-catalyzed silicone into designed molds, with the shape fitting the keys on the keyboard and having adequate ability to deform and recover. The electrodes were

DOI: 10.1021/acsnano.6b03926
ACS Nano XXXX, XXX, XXX−XXX

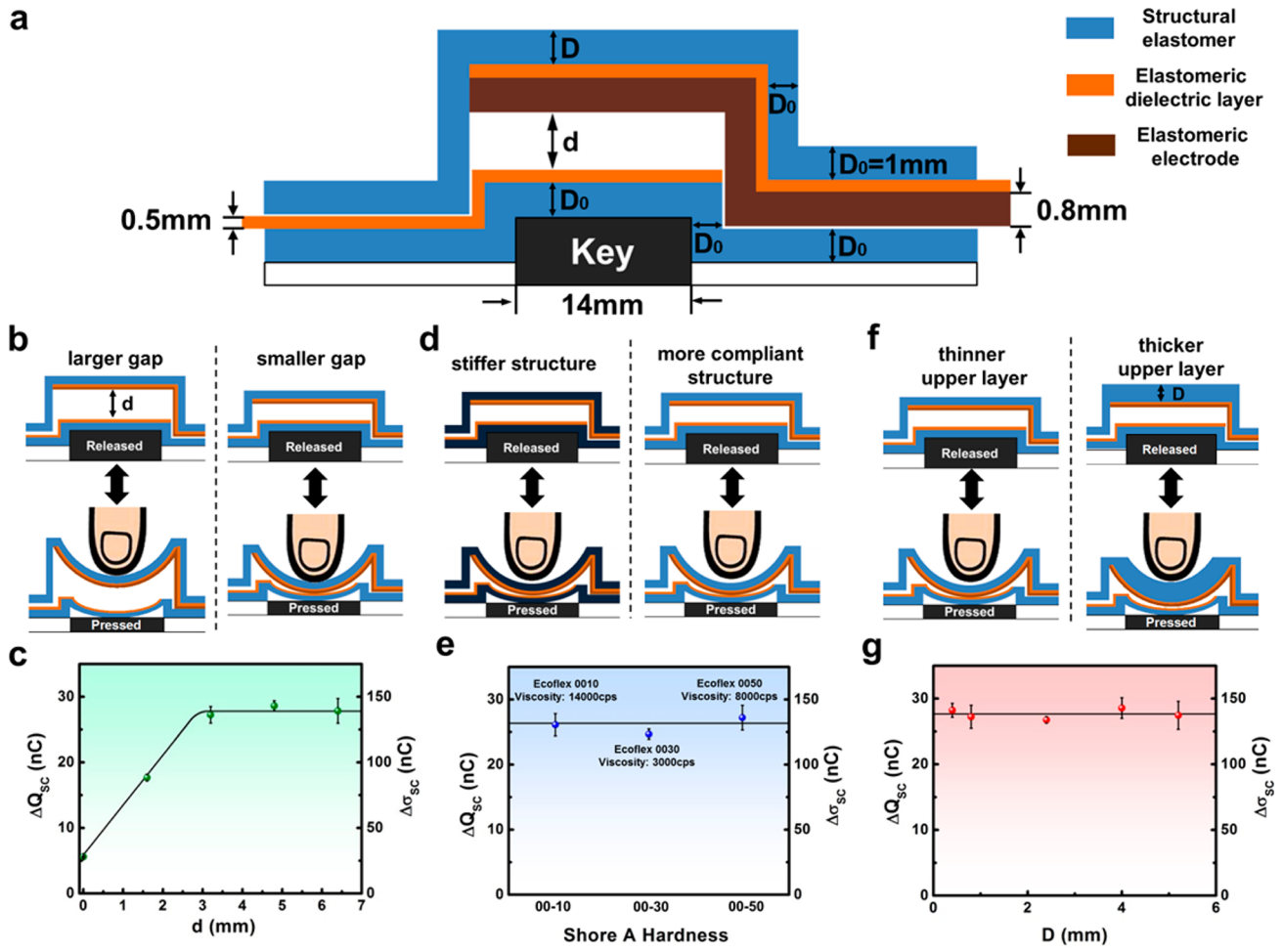

Figure 2. Electric outputs (short-circuit transferred charge amount ΔQ_{SC} and short-circuit transferred charge density $\Delta\sigma_{SC}$) of the elastomeric TENG with different structural parameters. (a) Schematic presenting the structure and dimensions of the TENG for one key. (b,c) Comparison schematics (b) and ΔQ_{SC} and $\Delta\sigma_{SC}$ (c) of TENGs with different gap distances. (d,e) Comparison schematics (d) and ΔQ_{SC} and $\Delta\sigma_{SC}$ (e) of TENGs with different structural materials (silicone with different cross-link density resulting in different shore A hardness and viscosity). (f,g) Comparison schematics (f) and ΔQ_{SC} and $\Delta\sigma_{SC}$ (g) of TENGs with top structural layer thicknesses.

conductive elastomeric films (~0.5 mm in thickness) fabricated by mixing the platinum-catalyzed silicone Ecoflex 0050 with carbon black and carbon nanotubes (CNTs) to ensure good flexibility, stretchability, and conductivity. The CNTs here not only served to help ensure the conductivity under strain but also enlarged the contact area by forming a nanostructured surface. The dielectric layer (~0.8 mm in thickness) was fabricated with the same material as the supporting top and bottom structures. Remarkably, for the cumulative effect of the contact-separation and the single-electrode working mode, the dielectric material (structural material) was selected to have a higher tendency to attract electrons (with its highest occupied energy state lower than that of both conductive materials) than both the electrode material and a human hand. Laminating these films together (with an air gap between the dielectric layer and the bottom electrode) in the order shown in Figure 1a, we manufactured a flexible and stretchable TENG for one single key solely by elastomeric layers.

The working principle of the as-fabricated TENG is schematically demonstrated in Figure 1b with five different states (states I–V). In the beginning, the finger is far away from the TENG and there is no deformation of the TENG, with both the surfaces of the TENG and the finger uncharged (state I). As the finger presses the key in full, contact electrification occurs in both the interface between the finger and the top dielectric surface and that between the dielectric layer and the bottom electrode. As a result of their differences in surface electron affinities, the skin and the bottom electrode will be positively charged, while their counter surfaces will be negatively charged (state II). As the pressing force is released, and the key returns to its original shape, a certain amount of charges (ΔQ_1) transfer from the bottom electrode to the top electrode, driven by their potential difference induced by the separation of triboelectric charges on both inner surfaces (state III). When the finger is fully removed from the top surface of the TENG, it will induce further change of potential difference between the two electrodes to drive another charge transfer with the amount of ΔQ_2 in the same direction (state IV). Later, when another typing is applied in the opposite sequence of states II–IV, the finger first touches the TENG again (state V) and presses onto the TENG to bring the two inner surfaces into full contact (state II). During these two steps, the charges will flow back in the opposite direction due to the reverse change of potential difference between the two electrodes, until it reaches state II to complete a full cycle of the energy conversion process. The dual-mode operation mechanism of the TENG plays a key role in enhancing its output performance, by adding up the amount of transferred charges

DOI: 10.1021/acsnano.6b03926
ACS Nano XXXX, XXX, XXX–XXX

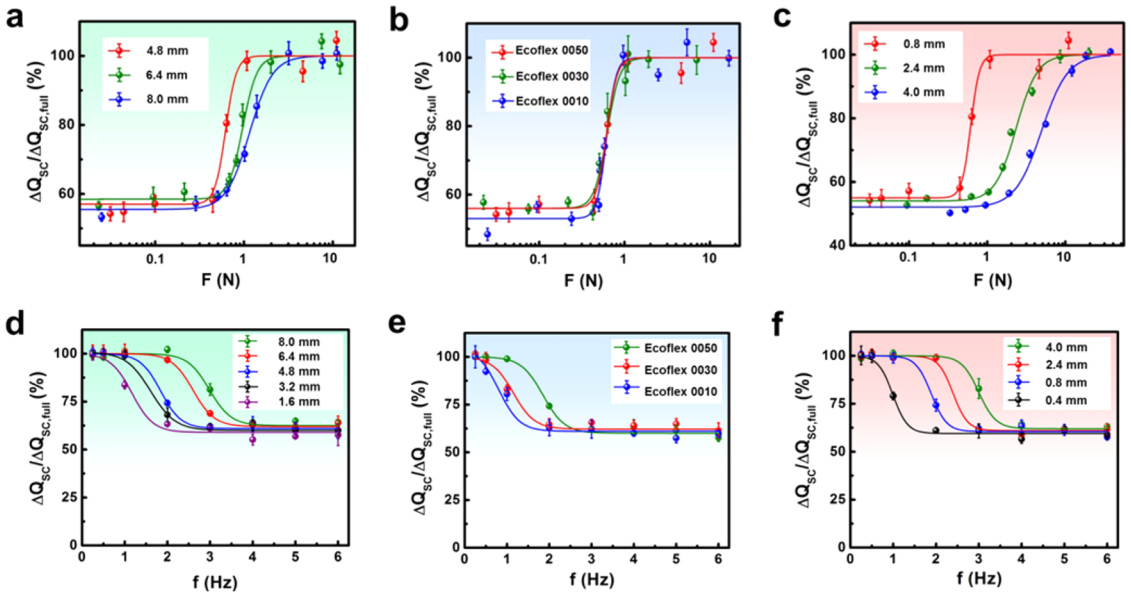

Figure 3. Electric outputs (short-circuit transferred charge amount ΔQ_{SC}) under different striking forces (F) and striking frequencies (f) of the elastomeric TENG with different structural parameters. (a–c) Normalized ΔQ_{SC}–F relationship between TENGs with different gap distances (a), structural materials with different hardness (b), and different top structural layer thicknesses (c). (d–f) Normalized ΔQ_{SC}–f relationship between TENGs with different gap distances (d), structural materials with different hardness (e), and different top structural layer thicknesses (f).

in two subsequent steps. Experiments were performed to confirm this dual-mode mechanism. In the experiments, we separated the typing operation into four sequential steps corresponding to the states in the working principle demonstrated in Figure 1b. Electric outputs have been proven as short-circuit charge transfer ΔQ_{SC} and open-circuit voltage (V_{OC}) in Figure 1c,d. From the ΔQ_{SC}–t curve, we could clearly observe the charge transfer $\pm\Delta Q_1$ and $\pm\Delta Q_2$ caused by the contact-separation mode and the single-electrode mode TENGs, with the ΔQ_2 about 20% of ΔQ_1. For the V_{OC}–t curve, the trend demonstrated in Figure 1d could also be explained by the theories of contact-separation TENG and single-electrode TENG. From state II to state III, the V_{OC} decreases for the first time due to the output of a contact-separation TENG. According to the theory of the contact-separation TENG, there is the relationship between the separation distance of two triboelectric charged layers ($x(t)$) and the open-circuit voltage (V_{OC}).[29,30]

$$V_{OC} = -\frac{Sx(t)}{\varepsilon_0} \quad (1)$$

where S is the contact area and ε_0 is the vacuum permittivity. In this way, with the increase of $x(t)$, there is the decrease of V_{OC} from 0 (here, we have the minus sign because the bottom electrode is grounded) for the first time due to the electric output of the contact-separation TENG. From state III to state IV, there is another reduction of V_{OC} because the absolute value of V_{OC} increases with the increase of $x_2(t)$ (separation distance between the hand and the TENG) theoretically for single-electrode TENG.[31] Later on, with the reverse charge transfer in the same amount from state IV to state II, V_{OC} increases with two steps in symmetry with the changes from state II to state IV.

The performance dependence of the TENG on various structural factors has been comprehensively studied to optimize its output performance. In this part, we pressed the TENG with the same finger every time to ensure full contact and well-controlled surface conditions. Here, we utilize the amount of transferred charges (ΔQ_{SC}) and the corresponding transferred charge density ($\Delta\sigma_{SC}$) in the short-circuit condition to evaluate the output performance of the TENG. These two values fundamentally determine the capability to charge the energy store unit by the TENG because the output power density is proportional to square of tribo-charge density.[32] In Figure 2a, the geometrical features that remain constant have been demonstrated. We first focused on the effect of air gap distance (d). The structural material was controlled to be Ecoflex 0050, and the top layer thickness (D) was 0.8 mm. The gap distances (d) were set to be 0, 1.6, 3.2, 4.8, and 6.4 mm. As shown in Figure 2b,c, with the increase of gap distance from 0 to 3.2 mm, there is an elevating trend of the ΔQ_{SC} (from ~5 to ~27.5 nC) and the $\Delta\sigma_{SC}$ (from ~25 to ~140 μC/m^2). From then on, the ΔQ_{SC} and the $\Delta\sigma_{SC}$ saturate at constant value. We also did a finite element simulation with COMSOL to show the above tendency, and the results (Figures S1 and S2) agree well with the experiment data. The reason is that when it comes to d = 0 mm, the output (ΔQ_{SC} = 5 nC) is solely caused by the single-electrode working mode since there is no air gap introduced. Later on, as demonstrated by the simulation result, the increase of the air gap distance contributes to the improvement of electric output for the contact-separation mode and has barely any influence on the single-electrode mode, rendering the above tendency. Next, we studied the influence of structural materials with different hardness and viscosity with constant d = 4.8 mm and D = 0.8 mm (Figure 2d,e). In this part, we used Ecoflex 0010, 0030, and 0050 (with shore A hardness of 00–10, 00–30, and 00–50 and viscosity of 14 000, 3000, and 8000 cps). As shown in Figure 2e, the ΔQ_{SC} and $\Delta\sigma_{SC}$ remain almost unchanged at ~27 nC and ~137 μC/m^2. The above results are reasonably consistent with theoretical expectation since the output of the contact-separation mode is not influenced by the change of structural material, and the change of the output for

DOI: 10.1021/acsnano.6b03926
ACS Nano XXXX, XXX, XXX–XXX

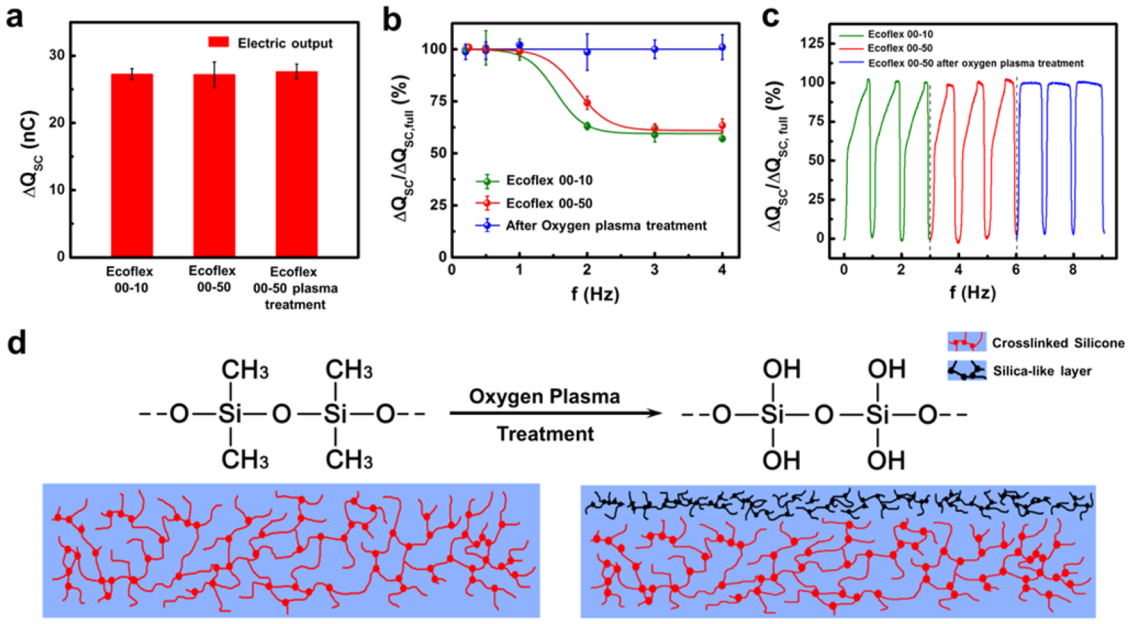

Figure 4. Experimental results to demonstrate the effects of dielectric materials onto electric outputs (ΔQ_{SC} and normalized ΔQ_{SC}) under different striking frequencies. (a) Comparison of ΔQ_{SC} between TENGs with Ecoflex 0010, Ecoflex 0050, and Ecoflex 0050 with oxygen plasma as the dielectric layer. (b) Comparison of normalized ΔQ_{SC} under different striking frequencies (f) between TENGs with Ecoflex 0010, Ecoflex 0050, and Ecoflex 0050 with oxygen plasma as the dielectric layer. (c) Output normalized ΔQ_{SC}–t curves of TENGs with Ecoflex 0010, Ecoflex 0050, and Ecoflex 0050 with oxygen plasma as the dielectric layer. (d) Schematic depicting the modification of silicone (Ecoflex 0050) after being treated with oxygen plasma.

the single-electrode mode is slight and only a small portion of the total output. Finally, we focused on the effect of the top-layer thickness (D), with d fixed at 4.8 mm and the structural material being Ecoflex 0050 (Figure 2f,g). As shown by the experimental results in Figure 2g, with the increase of D from 0.4 to 5.6 mm, the ΔQ_{SC} and the $\Delta\sigma_{SC}$ remained almost constant at ~27.5 nC and ~140 $\mu C/m^2$. According to simulation results (Figure S3), with D increasing from 0.4 to 5.6 mm, the electric output from the single-electrode TENG is reduced by only 10%. Considering that this only took up a small portion of the total electric output and that the contact-separation TENG is unaffected by the change of D, we find out that the experimental results agreed well with the simulation. One more thing worth noting from the above results is the ultrahigh transferred charge density ($\Delta\sigma_{SC}$ = 140 $\mu C/m^2$), which is among the highest values ever reported and the basis for high output power density.[32] The excellent transferred charge density could be attributed to both material selection and structural optimization. From the material's aspect, we know that only when the distance between two contacting surfaces is around intermolecular distance, will there be contact electrification caused by tunneling.[33,34] Therefore, the soft and highly flexible conductive and dielectric elastomers bring more surface into full contact (within the range of intermolecular distance) for triboelectrification because of their deformations during contact (in comparison with hard surfaces), with more tribo-charges accumulated on the same surface area. From the structural aspect, the outputs of dual modes could be added up, which is discussed above.

Next, we focused on optimizing the feasibility of the as-fabricated TENG to harvest biomechanical energy in real practice of typing. Here, the feature to deform with a smaller striking force and the feature to recover to the original shape rapidly after deformation were taken into consideration. Regarding the ability to deform, we measured the real-time striking forces (F) and ΔQ_{SC} simultaneously per striking cycle for TENGs with different gap distances (d), structural materials, and top layer thicknesses (D). The results are presented in Figure 3a–c by the ΔQ_{SC}–F_{peak} relationships. Here, the F_{peak} is the maximum striking force per cycle and is displayed in logarithmic scale on the x-axis, and the electric output values are displayed as normalized short-circuit transferred charge (normalized ΔQ_{SC}, with the ΔQ_{SC} divided by the constant maximum amount of transferred charge when the force was maximized) on the y-axis. As shown by the results of the experiments that research the effect of d (with D as 0.8 mm and Ecoflex 0050 as structural material, Figure 3a), TENG with larger d requires greater striking force for the same electric output, with F_{peak} being 0.8–1 N for the condition of d = 4.8 mm, 2–3 N for d = 6.4 mm, and 4–5 N for d = 8.0 mm to realize maximum ΔQ_{SC}. The reason is that a larger gap distance demands larger deformation for full contact and sufficient charge transfer, which in turn demands larger striking force. Next, we studied the effect of different structural materials (with d and D set as 4.8 and 0.8 mm). As demonstrated by Figure 3b, there is no remarkable difference in the curves of Ecoflex 0010, 0030, and 0050. Finally, we did experiments on TENGs with different D using the TENGs with d = 4.8 mm and with Ecoflex 0050 as the structural material. According to the curves shown in Figure 3c, TENGs with smaller top layer thickness (D) are easier to realize maximum electric output, which results from the lower ability for the thicker material to deform under the same striking force. On the other hand, we also compared the abilities of TENGs with different structural parameters to recover after deformation because the typing often proceeded continuously at a high frequency. To test this feature, we measured the ΔQ_{SC} of the TENGs under different striking frequencies (f). As shown in Figure 3d–f, the transferred charge amounts decrease to a certain level at higher frequencies. This is because the recovery speed of the TENG

DOI: 10.1021/acsnano.6b03926
ACS Nano XXXX, XXX, XXX–XXX

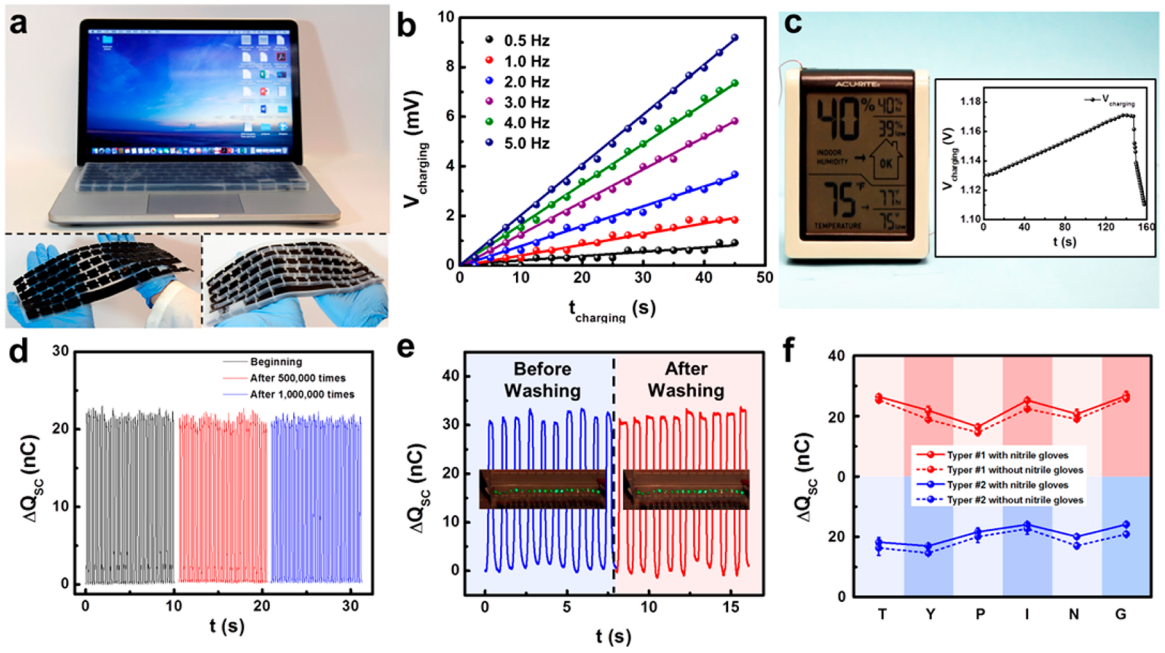

Figure 5. Output performances, applications, and characteristics of the as-fabricated keyboard cover based on the elastomeric TENG and the corresponding self-charging power system. (a) Photographs of the TENG-based keyboard cover. (b) Voltage of the energy storage unit (h-PPy-based supercapacitor) in the self-charging power system that is charged with the TENG stroke under different frequencies. (c) Photograph demonstrating that an electronic thermometer/hygrometer has been powered up with the energy harvested from typing at 6 Hz for 1 h on the TENG-based keyboard cover. The inset proves the switch point of voltage in order to drive the thermometer/hygrometer. (d) Results of long-term stability test of the TENG. (e) Electric outputs (ΔQ_{SC}) of the TENG-based keyboard cover before and after washing. The insets demonstrate its capability to power LEDs. (f) Electric outputs of two different operators typing the same word "TYPING" for five times continuously with/without wearing nitrile gloves on the TENG-based keyboard cover.

cannot compete with the deformation rate at high frequencies due to the high viscosity of the dielectric surface, rendering the reduction of the separation gap distance. According to the results, it can be found that the TENG with a larger gap distance, harder structural material, and thicker top layer demonstrates better high-frequency output performance, with ΔQ_{SC} deceasing more slowly at higher *f*. Combining the results of different striking forces and frequencies, we are convinced that there is the trade-off between shape deformation and recovery. Therefore, the moderate gap distance (4.8 mm) and top layer thickness (0.8 mm) with the Ecoflex 0050 as the structural material are applied in our design for better overall performance in practice. According to previous studies, the average typing force on the keyboard ranged from 1.84 N (little finger) to 3.33 N (thumb),[35] which means that the as-designed keyboard cover will not cause much resistance for typing.

Since the degradation of performance at high frequency may be attributed to the high viscosity of the elastomer surfaces, oxygen plasma treatment was applied on the dielectric surface to reduce this effect. In this regard, we carried out control experiments with the dielectric layer of (1) Ecoflex 0010, (2) Ecoflex 0050, and (3) Ecoflex 0050 with oxygen plasma treatment and measured their electric outputs under full contact for sufficient triboelectrification (ΔQ_{SC}) and their outputs (normalized ΔQ_{SC}) under multifrequencies. As shown by Figure 4a, there is no significant difference of maximum electric output (ΔQ_{SC}) between TENGs with the above three kinds of dielectric layers. On the other hand, the electric output performances under different frequencies of these devices largely differ from each other (Figure 4b,c). The TENG with Ecoflex 0050 as the dielectric material has an electric output (normalized ΔQ_{SC}) higher than that with Ecoflex 0010 when the pressing frequency is increased to 2 Hz, and both decrease to a low level with a further increase of the frequencies. In contrast, the TENG with the oxygen-plasma-treated dielectric layer performed excellent high-frequency electric outputs, for which the normalized ΔQ_{SC} remains constant even when the striking frequency is increased to 4 Hz. As shown by the curves in Figure 4c, there are significant slopes for Ecoflex 0010 and 0050 because of the recovery of the TENGs to their original shapes with a certain amount of time. This is due to the sticking of the dielectric layers to the electrode temporarily. However, no slope is observed from the curve after oxygen plasma treatment. In summary, from the comparisons between Ecoflex 0010 and Ecoflex 0050, it is proven that the increase of cross-link density of silicone may not affect the work function of the material significantly (Figure 4a). However, it influences the multifrequency output performance of the TENG by altering the viscosity of the silicone (Figure 4b,c). For the oxygen plasma treatment, we know that the surface-immobilized oxygen-enriched silicone groups may undergo a condensation reaction to form a silica-like layer with the thickness of several nanometers,[36,37] as shown in Figure 4d. Although this silica-like layer does not change the charge transfer behavior during contact electrification with an elastomeric electrode (Figure 4a), it had a viscosity much smaller than that of silicone. Therefore, the dielectric layer will not stick to the electrode after contact electrification, and the structure will recover to its original shape immediately (Figure 4b,c).

Here, we fabricated a keyboard-cover-shaped TENG based on the structural and material optimization discussed above (with d = 4.8 mm, D = 0.8 mm, Ecoflex 0050 as structural material and dielectric material, as well as dielectric layer treated with oxygen plasma). The bottom part (bottom structure and

DOI: 10.1021/acsnano.6b03926
ACS Nano XXXX, XXX, XXX−XXX

bottom electrode) and top part (top structure, top electrode, and dielectric layer) were fabricated separately and then stacked and sealed with Ecoflex 0050 to be a fully enclosed structure with an air gap in the middle (Figure 5a). The dependence of output power on loading resistance for the TENG on the top of one key has been studied. As demonstrated by Figure S4, at the loading resistance of ~250 MΩ, the TENG reaches the maximum instantaneous power density of ~300 mW/m^2 at a frequency of ~3 Hz. In order to harvest mechanical energy from typing, we built a self-charging power system to generate and store electricity simultaneously by integrating the TENG and a horn-like polypyrrole (hPPy)-based supercapacitor together (Figure S5). The properties of the supercapacitor are demonstrated in Figure S6. By typing on the keyboard continuously with different frequencies from 0.5 to 5.0 Hz, we have charged the supercapacitor to different voltage levels in the same time (45 s) (Figure 5b). The energy stored in this self-powered system was utilized to drive an electronic thermometer/hygrometer solely by energy harvested from the TENG-based keyboard cover through typing (Figure 5c). From the inset in Figure 5c, we confirm that when the voltage of the supercapacitor reached at ~1.15 V, the temperature and humidity meter began to work. In order to charge the supercapacitor to this level, the operator needs to type continuously for about 1 h with the typing frequency around 6 Hz with a corresponding average charging current ($I_{charging}$) around 0.3 μA, which is within the range of normal typing speeds in our daily lives. By that moment, nearly 8×10^{-4} J of electrical energy was stored in the supercapacitor. Charging the supercapacitor to ~1.6 V (for ~80 min) could power the thermometer/hygrometer for ~2 min (Figure S7). Moreover, to prove that the device can be sustained for a long period of time, we also performed a long-term stability test on one key. As shown in Figure 5d, the electric output (ΔQ_{SC}) remains unchanged after 1,000,000 operation cycles, which means that the keyboard cover could be used up to 1 year at least (given 2 h of typing everyday with the frequency of 4 Hz). This proves an excellent long-term stability of the device due to the soft and flexible elastomeric electrode and dielectric layer. Apart from the stability test, we also proceeded with experiments to demonstrate the water resistance of the keyboard cover. We measured the $\Delta Q_{SC,max}$ by pressing the letter "T" key before and after the keyboard cover was washed with water. The measurement was proceeded right after scrubbing the water off the TENG surface without waiting for the keyboard to completely dry. There was no significant declination in ΔQ_{SC} after washing, showing that the as-fabricated keyboard cover was not only washable but also insensitive to the surface conditions of the TENG itself (Figure 5e). Finally, we recorded the output performance (ΔQ_{SC}) of the TENG for different operators with/without wearing nitrile gloves while typing the same word "TYPING" continuously for five times (Figure 5f). Comparing the output performances between using a bare hand and wearing a nitrile glove for each operator, we could acquire similar "patterns" (with the condition of the bare hand being 2−3 nC smaller). On the other hand, when we compared the "pattern" for different operators, significant differences were observed due to distinct typing habits. Summarizing the results shown in Figure 5e,f and demonstrating the experimental results in Figure S8, we could see that the output performance (ΔQ_{SC}) is insensitive to both the TENG's surface condition and the operator's hand condition. That is because of the integration of the contact-separation mode TENG and the single-electrode mode TENG in this work. Due to the unaffected contact-separation TENG enclosed inside with its output amount almost 1 order larger than that of single-electrode TENG, the influence of the single-electrode TENG was largely reduced. In this way, the device becomes insensitive to both hand condition and device surface condition, showing that this device could be utilized to research the typing habits of different people by excluding the influence of environment and surface conditions such as humidity, oil, and sweat.

CONCLUSIONS

In summary, we have demonstrated a highly flexible TENG solely fabricated using elastomeric materials for harvesting biomechanical energy from a keyboard and buttons. Conductive elastomeric materials have been utilized as the triboelectric layers of TENG, and a dual-mode TENG is integrated with innovative structural design for achieving high energy conversion efficiency. In order to improve the feasibility of the TENG-based keyboard cover in practice (the capability of deforming and recovering more easily), the structural parameters (air gap distance and top layer thickness) have been optimized and the structural and dielectric materials have been rationally selected. Furthermore, oxygen plasma treatment has also been applied to the dielectric layer of the TENG for minimized viscosity. Finally, a keyboard cover based on all the above optimizations has been fabricated. It is integrated with an hPPy-based supercapacitor to build a self-charging power system. By typing on the keyboard for about 1 h, the energy storage unit could be charged to ~1.15 V with ~8×10^{-4} J electricity stored, which is enough to power up an electrical thermometer/hygrometer. The as-fabricated keyboard cover also performs high long-term stability and water resistance. In addition, due to the innovative structural design, the electric output of this TENG-based keyboard cover is insensitive to environmental and surface conditions, making it useful to research the typing habits of different operators.

METHODS

Fabrication of the Elastomeric Electrode. The liquid silicone rubber was obtained by mixing the silicone base and curing it with a volume ratio of 1:1 (Exoflex supersoft silicone 0010, 0030, and 0050 manufactured by Smooth-On, Inc.) in a beaker. Then we added the mixture of CB and CNTs (with a weight ratio of 2:1) into the beaker and stirred for uniform conductive silicone. The volume ratio between CB and Ecoflex is 1:1 (with a weight ratio of 1:13.4). Next, we smeared the mixture over a flat acrylic sheet (with the releasing agent poured on the surface in advance) at 30 °C for 6 h until the silicone was cured. Finally, we took it from the sheet and the elastomeric electrode could be obtained. The sheet resistance of the conductive elastomer is about 843 Ω without any strain.

Fabrication of the Dual-Mode All-Elastomer-Based TENG. The dielectric layer of the TENG was obtained by pouring mixed liquid silicone on the fabricated elastomeric conductive film and waiting for it to cure at 30 °C for 6 h. We utilized the "Hummer V" by Anatech for the oxygen plasma treatment for the dielectric layer. The dielectric layer was treated for 5 min at 4 V. For the structural layers, we manufactured the molds with acrylic sheets by processing them into different parts on the laser cutter and glued the parts together with epoxy. The liquid silicone was then poured inside the mold until it was cured. Finally, those layers were stacked together in the order shown in Figure 1a with the Ecoflex 0030 as the glue.

Fabrication of the Supercapacitor. The supercapacitor was fabricated to have a symmetrical structure. There are two identical hPPy electrodes as positive and negative electrodes with 1 M KCl aqueous solution as the electrolyte. The synthesis process of the hPPy

DOI: 10.1021/acsnano.6b03926
ACS Nano XXXX, XXX, XXX−XXX

is discussed below. The pyrrole monomer (Py, Capchem, 99%) was distilled twice in advance. The *p*-toluenesulfonic acid (TOSH, China Medicine Group, AR) and sodium *p*-toluenesulfonic acid (TOSNa, China Medicine Group, CP) were utilized in our synthesis. There are 300 mM pyrrole, 100 mM TOSH, and 400 mM TOSNa in the polymerization solution. Using a three-electrode cell with a titanium sheet as the working electrode and counter electrode and a saturated calomel electrode (SCE) as the reference electrode, the hPPy films were deposited on titanium electrodes by a pulse potentiostatic method, with a high potential of 0.75 V *vs* SCE, a high potential period of 0.04 s, a low potential of −0.2 V *vs* SCE, and a low potential period of 0.12 s as the parameters for the pulse. Next, the supercapacitor was packaged by two Kapton films and sealed with epoxy as the glue.

Electric Measurements. The short-circuit charge transfer and open-circuit voltage were measured by a Keithley 6514 system (Stanford Research System). During the measurements in Figures 3 and 4b,c, the TENG was stroked by a mass (~14 × 14 mm^2 in surface area) on a linear motor with the strokes triggered by the linear motion of the motor. During the measurement in Figure 5d, the TENG was stroked by the same mass on a Labworks ET-126 shaker with the strokes triggered by the shaking motion.

ASSOCIATED CONTENT

Supporting Information

The Supporting Information is available free of charge on the ACS Publications website at DOI: 10.1021/acsnano.6b03926.

Additional experimental details and figures (PDF)
Movie S1 (AVI)
Movie S2 (AVI)

AUTHOR INFORMATION

Corresponding Author

*E-mail: zhong.wang@mse.gatech.edu.

Author Contributions

⊥S.L., W.P., and J.W. contributed equally.

Notes

The authors declare no competing financial interest.

ACKNOWLEDGMENTS

This research was supported by the Hightower Chair Foundation, the "Thousands Talents" program for a pioneer researcher and his innovation team and National Natural Science Foundation of China (21274115).

REFERENCES

(1) O'Regan, B.; Gratzel, M. A Low-Cost, High-Efficiency Solar Cell Based on Dye-Sensitized. *Nature* **1991**, *353*, 737−740.
(2) Huynh, W. U.; Dittmer, J. J.; Alivisatos, A. P. Hybrid Nanorod-Polymer Solar Cells. *Science* **2002**, *295*, 2425−2427.
(3) Bach, U.; Lupo, D.; Comte, P.; Moser, J. E.; Weissörtel, F.; Salbeck, J.; Spreitzer, H.; Grätzel, M. Solid-State Dye-Sensitized Mesoporous TiO_2 Solar Cells with High Photon-to-Electron Conversion Efficiencies. *Nature* **1998**, *395*, 583−585.
(4) Dresselhaus, M. S.; Chen, G.; Tang, M. Y.; Yang, R. G.; Lee, H.; Wang, D. Z.; Ren, Z. F.; Fleurial, J. P.; Gogna, P. New Directions for Low-Dimensional Thermoelectric Materials. *Adv. Mater.* **2007**, *19*, 1043−1053.
(5) Wang, Z. L.; Song, J. H. Piezoelectric Nanogenerators Based on Zinc Oxide Nanowire Arrays. *Science* **2006**, *312*, 242−246.
(6) Wang, Z. L.; Wu, W. Nanotechnology-Enabled Energy Harvesting for Self-Powered Micro-/Nanosystems. *Angew. Chem., Int. Ed.* **2012**, *51*, 11700−11721.
(7) Arico, A. S.; Bruce, P.; Scrosati, B.; Tarascon, J. M.; van Schalkwijk, W. Nanostructured Materials for Advanced Energy Conversion and Storage Devices. *Nat. Mater.* **2005**, *4*, 366−377.
(8) Paradiso, J. A.; Starner, T. Energy Scavenging for Mobile and Wireless Electronics. *IEEE Pervasive Comput.* **2005**, *4*, 18−27.
(9) Xu, S.; Qin, Y.; Xu, C.; Wei, Y.; Yang, R.; Wang, Z. L. Self-Powered Nanowire Devices. *Nat. Nanotechnol.* **2010**, *5*, 366−373.
(10) Wang, Z. L.; Wang, X. Nanogenerators and Piezotronics. *Nano Energy* **2015**, *14*, 1−2.
(11) Wang, Z. L. Triboelectric Nanogenerators as New Energy Technology for Self-Powered Systems and as Active Mechanical and Chemical Sensors. *ACS Nano* **2013**, *7*, 9533−9557.
(12) Beeby, S. P.; Torah, R. N.; Tudor, M. J.; Glynne-Jones, P.; O'Donnell, T.; Saha, C. R.; Roy, S. A Micro Electromagnetic Generator for Vibration Energy Harvesting. *J. Micromech. Microeng.* **2007**, *17*, 1257.
(13) Sari, I.; Balkan, T.; Kulah, H. An Electromagnetic Micro Power Generator for Wideband Environmental Vibrations. *Sens. Actuators, A* **2008**, *145−146*, 405−413.
(14) Mitcheson, P. D.; Miao, P.; Stark, B. H.; Yeatman, E. M.; Holmes, A. S.; Green, T. C. MEMS Electrostatic Micropower Generator for Low Frequency Operation. *Sens. Actuators, A* **2004**, *115*, 523−529.
(15) Jiang, T.; Zhang, L. M.; Chen, X.; Han, C. B.; Tang, W.; Zhang, C.; Xu, L.; Wang, Z. L. Structural Optimization of Triboelectric Nanogenerator for Harvesting Water Wave Energy. *ACS Nano* **2015**, *9*, 12562−12572.
(16) Li, S.; Wang, S.; Zi, Y.; Wen, Z.; Lin, L.; Zhang, G.; Wang, Z. L. Largely Improving the Robustness and Lifetime of Triboelectric Nanogenerators through Automatic Transition between Contact and Noncontact Working States. *ACS Nano* **2015**, *9*, 7479−7487.
(17) Chen, J.; Yang, J.; Li, Z.; Fan, X.; Zi, Y.; Jing, Q.; Guo, H.; Wen, Z.; Pradel, K. C.; Niu, S.; Wang, Z. L. Networks of Triboelectric Nanogenerators for Harvesting Water Wave Energy: a Potential Approach Toward Blue Energy. *ACS Nano* **2015**, *9*, 3324−3331.
(18) Guo, H.; Wen, Z.; Zi, Y.; Yeh, M. H.; Wang, J.; Zhu, L.; Hu, C.; Wang, Z. L. A Water-Proof Triboelectric-Electromagnetic Hybrid Generator for Energy Harvesting in Harsh Environments. *Adv. Energy Mater.* **2016**, *6*, 1501593.
(19) Wang, S.; Lin, L.; Wang, Z. L. Nanoscale Triboelectric-Effect-Enabled Energy Conversion for Sustainably Powering Portable Electronics. *Nano Lett.* **2012**, *12*, 6339−6346.
(20) Bai, P.; Zhu, G.; Lin, Z. H.; Jing, Q.; Chen, J.; Zhang, G.; Ma, J.; Wang, Z. L. Integrated Multilayered Triboelectric Nanogenerator for Harvesting Biomechanical Energy from Human Motions. *ACS Nano* **2013**, *7*, 3713−3719.
(21) Wang, J.; Li, X.; Zi, Y.; Wang, S.; Li, Z.; Zheng, L.; Yi, F.; Li, S.; Wang, Z. L. A Flexible Fiber-Based Supercapacitor-Triboelectric-Nanogenerator Power System for Wearable Electronics. *Adv. Mater.* **2015**, *27*, 4830−4836.
(22) Zi, Y.; Wang, J.; Wang, S.; Li, S.; Wen, Z.; Guo, H.; Wang, Z. L. Effective Energy Storage from a Triboelectric Nanogenerator. *Nat. Commun.* **2016**, *7*, 10987.
(23) Wang, S.; Zi, Y.; Zhou, Y. S.; Li, S.; Fan, F.; Lin, L.; Wang, Z. L. Molecular Surface Functionalization to Enhance the Power Output of Triboelectric Nanogenerators. *J. Mater. Chem. A* **2016**, *4*, 3728−3734.
(24) Wang, S.; Xie, Y.; Niu, S.; Lin, L.; Wang, Z. L. Freestanding Triboelectric-Layer-Based Nanogenerators for Harvesting Energy from a Moving Object or Human Motion in Contact and Non-Contact Modes. *Adv. Mater.* **2014**, *26*, 2818−2824.
(25) Zhu, G.; Chen, J.; Zhang, T.; Jing, Q.; Wang, Z. L. Radial-Arrayed Rotary Electrification for High Performance Triboelectric Generator. *Nat. Commun.* **2014**, *5*, 3426.
(26) Wang, J.; Wen, Z.; Zi, Y.; Lin, L.; Wu, C.; Guo, H.; Xi, Y.; Xu, Y.; Wang, Z. L. Self-Powered Electrochemical Synthesis of Polypyrrole from the Pulsed Output of a Triboelectric Nanogenerator as a Sustainable Energy System. *Adv. Funct. Mater.* **2016**, *26*, 3542−3548.
(27) Löwe, C.; Zhang, X.; Kovacs, G. Elastomers in Actuator Technology. *Adv. Eng. Mater.* **2005**, *7*, 361−367.
(28) Rogers, J. A.; Someya, T.; Huang, Y. Materials and Mechanics for Stretchable Electronics. *Science* **2010**, *327*, 1603−1607.

DOI: 10.1021/acsnano.6b03926
ACS Nano XXXX, XXX, XXX−XXX

(29) Niu, S.; Wang, Z. L. Theoretical Systems of Triboelectric Nanogenerators. *Nano Energy* **2015**, *14*, 161−192.
(30) Niu, S.; Wang, S.; Lin, L.; Liu, Y.; Zhou, Y. S.; Hu, Y.; Wang, Z. L. Theoretical Study of Contact-Mode Triboelectric Nanogenerators as an Effective Power Source. *Energy Environ. Sci.* **2013**, *6*, 3576−3583.
(31) Niu, S.; Liu, Y.; Wang, S.; Lin, L.; Zhou, Y. S.; Hu, Y.; Wang, Z. L. Theoretical Investigation and Structural Optimization of Single-Electrode Triboelectric Nanogenerators. *Adv. Funct. Mater.* **2014**, *24*, 3332−3340.
(32) Zi, Y.; Niu, S.; Wang, J.; Wen, Z.; Tang, W.; Wang, Z. L. Standards and Figure-of-Merits for Quantifying the Performance of Triboelectric Nanogenerators. *Nat. Commun.* **2015**, *6*, 8376.
(33) Li, S.; Zhou, Y.; Zi, Y.; Zhang, G.; Wang, Z. L. Excluding Contact Electrification in Surface Potential Measurement Using Kelvin Probe Force Microscopy. *ACS Nano* **2016**, *10*, 2528−2535.
(34) Zhou, Y. S.; Liu, Y.; Zhu, G.; Lin, Z. H.; Pan, C.; Jing, Q.; Wang, Z. L. *In Situ* Quantitative Study of Nanoscale Triboelectrification and Patterning. *Nano Lett.* **2013**, *13*, 2771−2776.
(35) Martin, B. J.; Armstrong, T. J.; Foulke, J. A.; Natarajan, S.; Klinenberg, E.; Serina, E.; Rempel, D. Keyboard Reaction Force and Finger Flexor Electromyograms During Computer Keyboard Work. *Hum. Factors* **1996**, *38*, 654−664.
(36) Özçam, A. E.; Efimenko, K.; Genzer, J. Effect of Ultraviolet/Ozone Treatment on the Surface and Bulk Properties of Poly(Dimethyl Siloxane) and Poly(Vinylmethyl Siloxane) Networks. *Polymer* **2014**, *55*, 3107−3119.
(37) Efimenko, K.; Wallace, W. E.; Genzer, J. Genzer, Surface Modification of Sylgard-184 Poly(Dimethyl Siloxane) Networks by Ultraviolet and Ultraviolet/Ozone Treatment. *J. Colloid Interface Sci.* **2002**, *254*, 306−315.

DOI: 10.1021/acsnano.6b03926
ACS Nano XXXX, XXX, XXX−XXX